Proceedings World Geothermal Congress 2023
Beijing, China, April 17 – 21, 2023

A Unified Model for Predicting Barite Scale Inhibition at the Conditions of Geothermal Productions

Yue Zhao, Yiming An, Jinhua Wang, Fei Sun, Song Gao, Xiaoping Fu, Hui Wang

SINOPEC Research Institute of Petroleum Processing Co., Ltd., Beijing 100083, China

zhaoy.ripp@sinopec.com

Keywords: Barite, induction time, crystallization model, inhibition model, geothermal conditions

ABSTRACT

Barite scaling problem is ubiquitous during geothermal productions. It may cause significant economic loss if being treated improperly. Adding threshold scale inhibitors is one of the most efficient ways to control the barite scale. However, no quantitative studies have been conducted to predict the severity of the barite scale problem during geothermal production and estimate the inhibitor concentration needed for scaling control. In this study, the induction times of barite at the experimental ranges of barite saturation index (*SI*) 1.7 – 2.1, temperature (*T*) 50°C to 90°C, 0.2 mol/L NaCl and 0.01 mol/L Ca^{2+} without and with the scale inhibitor polyepoxysuecinic acid (PESA) were measured by a novel laser apparatus. Based on the experimental results, a new barite crystallization and inhibition model has been established. The predicted results show good agreements with the experimental data, indicating the validity of the model developed. With this model, the minimum scale inhibitor concentration needed during the industrial processes can be predicted, and a better barite scale management during geothermal productions can be achieved.

1. INTRODUCTION

Mineral scale formation can be commonly discovered in several industrial processes, such as water treatment (Peiris et al., 2013; Zhang et al., 2014; Di Lorenzo et al., 2020; Huang et al., 2020), oil and gas production (Cowan and Weintritt, 1976; Oddo and Tomson, 1994; Kan and Tomson, 2012) and geothermal production (Orywall et al., 2017; Griffiths et al., 2016; Bozau et al., 2015; Tranter et al., 2021). In geothermal productions, mineral scaling could cause significant problems by damaging heat exchange units, blocking pipelines and reducing injectivity, resulting in the rising challenges for the long-term utilization (Genter et al., 1996; Dezayes et al., 2010). Among several different types of minerals, barite is one of the most troublesome scales formed during the geothermal productions since it is difficult to remove both physically and chemically (Yan et al., 2015). One of the most economic and effective methods to control barite scale during geothermal productions is adding only a few mg/L, or lower, of threshold scale inhibitors (Zhang et al., 2018). Therefore, it is critical to predict the barite crystallization kinetics accurately to evaluate the severity of the barite scaling problems in the geothermal wells. Also, the barite crystallization kinetics with different scale inhibitors should also be qualitatively investigated to help industry improve the scale management strategy.

The nucleation and crystal growth of barite mineral has been extensively investigated in the previous studies (Dai et al., 2016; Risthaus et al., 2001; Sánchez-Pastor et al., 2006; Kowacz et al., 2007; Pina et al., 1998; Bracco et al., 2016). The combination of the two is called the crystallization process. An experimental concept of induction time (t_{ind}) defined by Söhnel and Mullin (1988) can be used to evaluate the overall crystallization kinetics of the mineral scale (Söhnel and Mullin, 1988). The definition of t_{ind} is the time interval between the beginning of the supersaturation and the crystal detected.

Several studies have implied the t_{ind} to investigate the crystallization and inhibition kinetics of the barite scale during oil and gas production (He et al., 1996; Xiao et al., 2001; Dai et al., 2019; Dai et al., 2020). However, the t_{ind} has not been applied to the barite crystallization and inhibition kinetics studies at the geothermal productions. In this study, the crystallization and inhibition t_{ind} of barite is measured at the conditions of barite saturation index (*SI*) 1.7 – 2.1, temperature (*T*) 50°C to 90°C with 0.2 mol/L NaCl and 0.01 mol/L Ca^{2+} to mimic the geothermal production conditions. Based on the experimental results, a semiempirical model is developed to predict the barite crystallization and inhibition kinetics in the geothermal produced water. The model can also be used to predict the minimum scale inhibitor concentration needed to control the barite scale during geothermal production by calculating the inhibitor concentration needed when t_{ind} equals the retention time of the produced water. The model developed in this study could provide a more efficient scale management strategy to geothermal industry while reducing the chemical cost.

2. METHODS

2.1 Static Jar Test for Inhibitor Screening

Static jar tests are firstly used in this study to screen the most effective chemical for barite inhibition. During the experiments, the 125 mL of solution with 7500 mg/L NaCl, 660 mg/L $BaCl_2 \cdot 2H_2O$ as well as different types and concentrations of scale inhibitors were firstly introduced into the reaction jars. The six inhibitors tested are polyepoxysuecinic acid (PESA), 1-hydroxyethylidene-1,1-diphosphonic acid (HEDP), 2-phosphonobutane -1,2,4-tricarboxylic acid (PBTC), acrylic acid-2-acrylamido-2-methylpropyl sulfonic acid copolymer (AA/AMPS), amino trimethylene phosphonic acid (ATMP) and ethylenediaminetetra(methylene phosphonic acid) (EDTMP), all of which are commercially available. Then, the solutions with 7500 mg/L NaCl and 800 mg/L Na_2SO_4 were also introduced into the reaction jars. All the mixed solutions were put into the water bath at the temperature of 70°C for reaction. After 10 hr experiments, the solutions were immediately filtered with the filter paper. The filtered solutions were used to measure Ba^{2+} concentration with ICP-OES after the reactions.

2.2 Kinetic Turbidity Test Method with Laser Apparatus

After selecting the most effective inhibitor at the experimental conditions, the laser apparatus was used to measure the induction time (t_{ind}) of barite crystallization and inhibition with the inhibitor under different barite saturation index (*SI*), temperature, and inhibitor concentration conditions. The diagram of the laser apparatus is shown in Figure 1. The temperature is controlled with a water both, and the solution is continuous mixed by a stirring bar. A green laser penetrates through the reaction solution and is received by a Si photodiode. The receiver transmits the laser signal into the electric current, which can be recorded by a multimeter. When the green laser is scattered by the crystals forming in the reaction solution, the recorded electric current would also decrease. The time taken for the recorded signal begins to drop is called the t_{ind}. The t_{ind} measured in the absence and presence of the scale inhibitor is used to evaluate the barite crystallization and inhibition kinetics and develop the model accordingly.

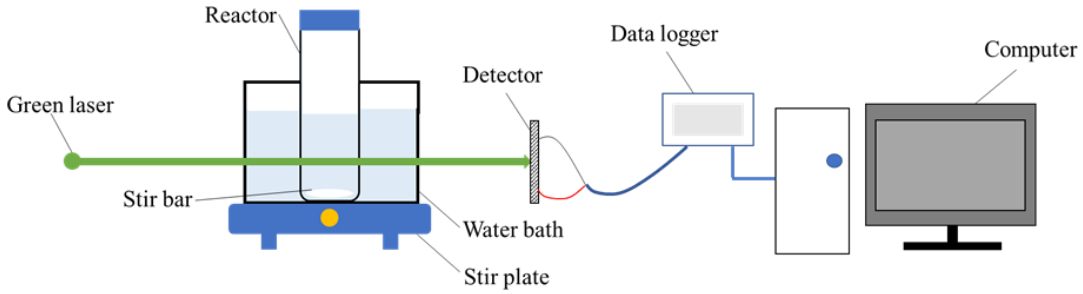

Figure 1: The diagram of the laser apparatus

The reaction solutions used in the kinetic turbidity test were made by the mixing of cationic (with Ba^{2+}) and anionic solutions (with SO_4^{2-}). Both solutions contained 0.2 M NaCl, 0.01 M Ca^{2+} and 100 mM 1,4-Piperazinediethanesulfonic acid (PIPEs) to mimic the water composition of the formation waters exploited from the geothermal wells. The concentrations of NaCl and Ca^{2+} are selected as the 50 percentile of the collected water compositions data of fluids in the geothermal wells in China. The Ba^{2+} and SO_4^{2-} concentrations in cationic and anionic solutions under different experimental conditions are shown in Table 1. The *SI* of barite is calculated by PHREEQC. In these experiments, the molar ratio of $[Ba^{2+}]/[SO_4^{2-}] = 1$. The conditions are chosen for the most severe barite scaling condition at a fixed barite *SI* (He et al., 1994). When conducting the kinetic turbidity test, 10 mL cationic solution without or with the scale inhibitors was firstly introduced into the reaction bottle of the laser apparatus for preheating. The experiment begins as soon as the preheated anionic solution was also introduced into the reactor.

Table 2: The experimental conditions designed for kinetic turbidity tests with laser apparatus

T (℃)	$[Ba^{2+}]$ (mM)	$[SO_4^{2-}]$ (mM)	Barite *SI*	*T* (℃)	$[Ba^{2+}]$ (mM)	$[SO_4^{2-}]$ (mM)	Barite *SI*
50	0.5534	0.5534	1.8	70	0.7622	0.7622	1.9
50	0.6219	0.6219	1.9	70	0.8563	0.8563	2.0
50	0.6985	0.6985	2.0	90	0.6854	0.6854	1.7
50	0.7846	0.7846	2.1	90	0.7700	0.7700	1.8
70	0.6785	0.6785	1.8	90	0.8652	0.8652	1.9

3. RESULTS AND DISCUSSIONS

3.1 Inhibitor screening results

With the method described in section 2.1, the barite inhibition efficiencies of PESA, HEDP, PBTC, AA/AMPS, ATMP and EDTMP are tested. The inhibition efficiency of barite in the static bar tests can be calculated as follows:

$$Inhibition\ efficiency = \frac{[Ba^{2+}]_{awi} - [Ba^{2+}]_{awoi}}{([Ba^{2+}]_b - [Ba^{2+}]_{awoi})} \quad (1)$$

where $[Ba^{2+}]_{awi}$ represents Ba^{2+} concentration after the experiments with inhibitor; $[Ba^{2+}]_{awoi}$ represents Ba^{2+} concentration after the experiments without inhibitor; and $[Ba^{2+}]_b$ represents Ba^{2+} concentration before the experiments. Based on the calculation results, the barite inhibition efficiencies of 6 different inhibitors are shown in Figure 2. The results indicate that at the experimental conditions, PESA shows the best performance among the 6 inhibitors selected. In the following studies, the barite inhibition model will be firstly developed for PESA.

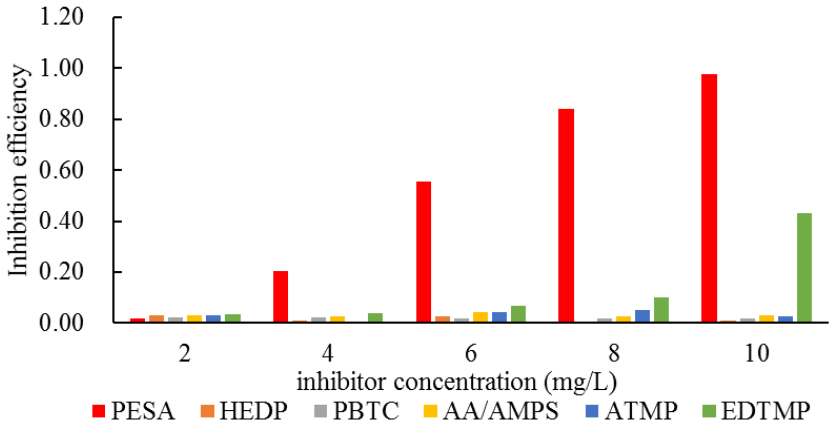

Figure 2: The inhibition efficiencies of PESA, HEDP, PBTC, AA/AMPS, ATMP and EDTMP on barite at different concentrations

3.2 Barite crystallization model

The barite crystallization kinetics is evaluated with the experimental method shown in section 2.2 by measuring the t_{ind} of the barite crystallization without inhibitors (t_0). The results are shown in Table 2.

Table 2: The t_{ind} of barite crystallization under different barite *SI* and *T* conditions

T (℃)	Barite *SI*	t_{ind} (s)	*T* (℃)	Barite *SI*	t_{ind} (s)
50	1.8	35	70	1.9	14
50	1.9	25	70	2.0	9
50	2.0	19	90	1.7	16
50	2.1	11	90	1.8	12
70	1.8	20	90	1.9	8

3.2.1 Effect of *SI* on barite crystallization

The effect of *SI* on the t_{ind} of barite crystallization are analyzed by plotting $log_{10}t_{ind}$ versus barite *SI* at the same temperature. The analysis results are shown in Figure 3. The results indicate that at a fixed temperature, the logarithm of the barite crystallization t_{ind} decrease linearly with the increase of barite *SI* with the slope of -1.6221 ± 0.1145.

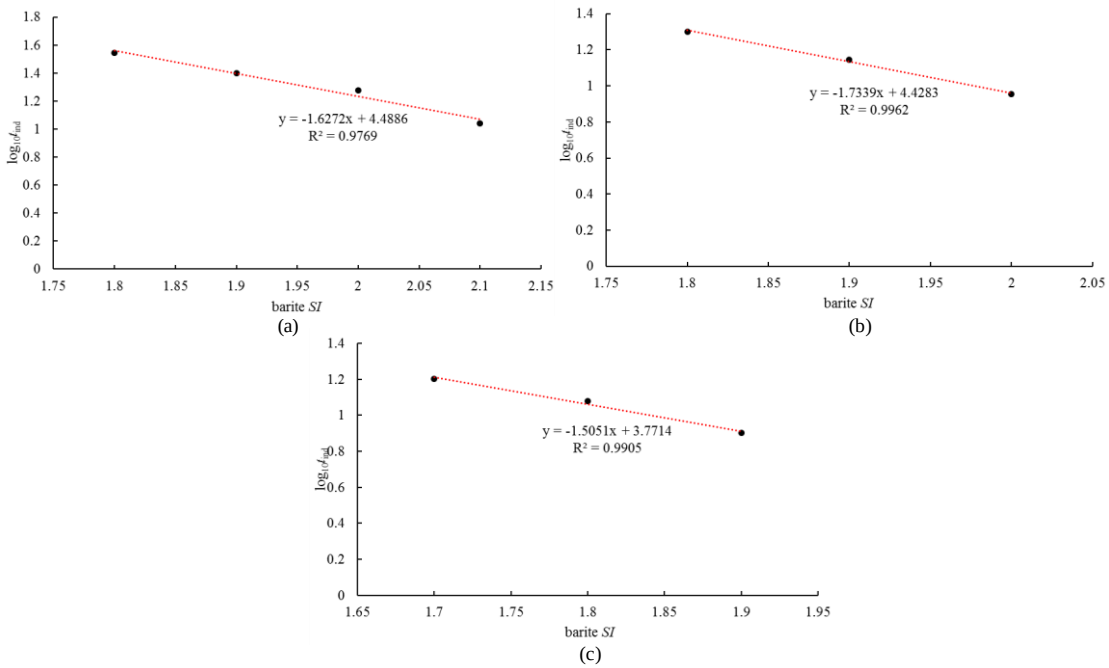

Figure 3: The effect of barite *SI* on barite crystallization rate at (a) *T* = 50℃, (b) *T* = 70℃ and (c) *T* = 90℃ conditions

3.2.2 Effect of *T* on barite crystallization

The effect of *T* on the t_{ind} of barite crystallization is also analyzed by plotting $log_{10}t_{ind}$ versus 1/*T*(K) at the fixed barite *SI*. According to Arrhenius equation, the logarithm of the reaction kinetics shows linear relationship with 1/*T*(K). Therefore, in this study, the relationship between the $log_{10}t_{ind}$ and 1/*T*(K), instead of *T*(K), is also evaluated. The analysis results are shown in Figure 4. The results indicate that at certain barite *SI*, the linear dependence of $log_{10}t_{ind}$ and 1/*T*(K) can be found with the slope of 1404.7 ± 64.9.

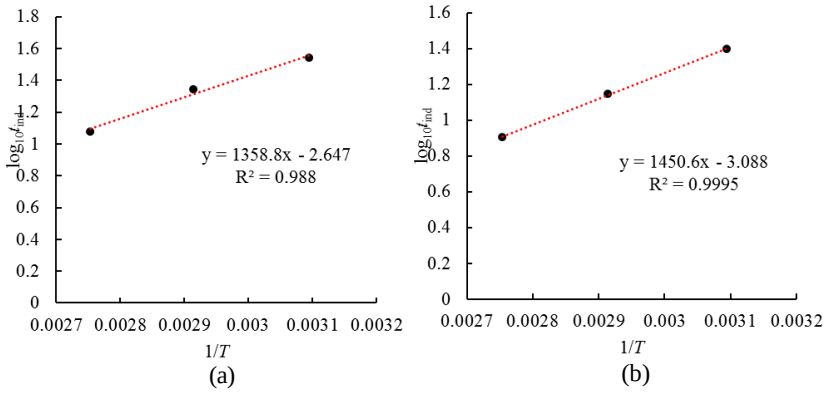

Figure 4: The effect of *T*(K) on barite crystallization rate at (a) barite *SI* = 1.8 and (b) barite *SI* = 1.9 conditions

3.2.3 Barite crystallization model development

With the discussions in section 3.2.1 and 3.2.2, the barite crystallization kinetic model can be expressed as:

$$log_{10}t_0 = a_1 \times SI + \frac{a_2}{T(K)} + a_3 \quad (2)$$

After fitting equation 2 with the experimental data shown in Table 2 by Origin, the parameters are determined as follows with the R^2 of 0.9836:

$$log_{10}t_0 = -1.6597 \times SI + \frac{1468.5195}{T(K)} + 0.0112 \quad (3)$$

By using equation 3, the barite crystallization kinetics can be determined by knowing the barite *SI* and *T*. The barite crystallization model (equation 3) is evaluated in Figure 5 by comparing the measured $\log_{10}t_{ind}$ with the calculated $\log_{10}t_{ind}$. The evaluation results show that the errors between the measured and calculated results are less than ± 0.05, indicating that the barite crystallization model developed in this study can be applied to estimate the severity of barite scaling problems with no inhibitors.

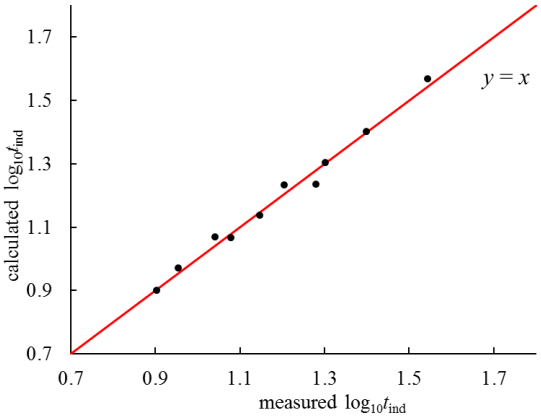

Figure 5: Evaluation of barite crystallization model at the conditions of barite *SI* 1.7 to 2.1 and *T* 50 to 90°C conditions. Red line: *y* = *x*. The linear fitting result of the black dots: *y* = 1.0034*x*, R^2 = 0.9879.

3.3 Barite inhibition model

After choosing PESA as the target scale inhibitor to develop barite crystallization and inhibition models in section 3.1, the t_{ind} of barite with PESA are also measured to develop the inhibition model. The results show that the logarithm of induction times with inhibitor (t_{inh}) increase linearly with the inhibitor concentrations ([Inhibitor]) at the certain *T* and *SI* condition. The detailed experimental results are shown in Table 3.

Table 3: The t_{ind} of barite inhibition (t_{inh}) with PESA under different barite *SI*, and *T* and inhibitor concentration

T (℃)	SI	[Inhibitor] (mg/L)	t_{inh} (s)	$\log_{10}t_{inh}$	Slope of $\log_{10}\frac{t_{inh}}{t_0}$ vs. [Inhibitor]	R^2
50	1.9	0	25	1.398	4.8114	0.9972
50	1.9	0.2	323	2.509		
50	1.9	0.3	642	2.808		
50	1.9	0.5	5812	3.764		
50	2	0	19	1.279	3.0135	0.9994
50	2	0.2	89	1.949		
50	2	0.5	597	2.776		
50	2	0.8	4770	3.679		
50	2.1	0	11	1.041	2.1904	0.9962
50	2.1	0.5	144	2.158		
50	2.1	1	1043	3.018		
50	2.1	1.5	28975	4.462		
70	1.8	0	20	1.301	4.2200	0.9955
70	1.8	0.2	131	2.117		
70	1.8	0.3	266	2.425		
70	1.8	0.5	3217	3.507		
70	1.9	0	14	1.146	2.7879	0.9974
70	1.9	0.2	68	1.833		
70	1.9	0.5	279	2.446		
70	1.9	1	9025	3.955		
70	2	0	9	0.954	1.3008	0.9988
70	2	0.5	34	1.531		
70	2	1.5	1021	3.009		
70	2	2.5	14409	4.159		
90	1.7	0	16	1.204	3.2197	0.9992
90	1.7	0.2	59	1.771		
90	1.7	0.5	578	2.762		
90	1.7	1	29191	4.465		
90	1.8	0	12	1.079	2.3205	0.9946
90	1.8	0.5	129	2.111		
90	1.8	1	1723	3.236		
90	1.8	1.2	11316	4.054		
90	1.9	0	8	0.903	1.8031	0.9999
90	1.9	0.5	67	1.826		
90	1.9	1	504	2.702		
90	1.9	1.5	4009	3.603		

The slope of $log_{10}\frac{t_{inh}}{t_0}$ vs. inhibitor concentration is defined as k_{inh}. Therefore, the relationship between t_{inh} and the concentration of inhibitor can be expressed as:

$$log_{10}\frac{t_{inh}}{t_0} = k_{inh} \times [Inhibitor] \tag{4}$$

The parameter k_{inh} is also a function of reaction T and barite SI. After fitting the different forms of equations with the experimental data, the expression of k_{inh} is determined as:

$$k_{inh} = \frac{1072.7286}{T(K)} + \frac{13488.6875}{SI \times T(K)} - 21.2048 \tag{5}$$

With equation 4 and 5, the t_{ind} of barite inhibition with PESA can be calculated by knowing the water compositions and reaction temperature. The validity of the inhibition model is evaluated with the experimental data. The comparison results shown in Figure 6 illustrate that the errors between the measured $\log_{10}t_{ind}$ and the calculated $\log_{10}t_{ind}$ with the absence and presence of the scale inhibitor PESA are less than ± 0.5. It implies the barite inhibition model (equation 4 and 5) developed can be used to predict the induction time of scale formation with and without scale inhibitors. Several studies investigated that when the induction time is longer than the retention time of geothermal produced water, the scaling tends not to form (Dai et al., 2019; Dai et al., 2020). Therefore, by knowing the retention time of the produced water, the minimum scale inhibitor concentration needed to prevent scaling can also be calculated by the barite crystallization and inhibition model developed in this study. To conclude, this barite crystallization and inhibition model could not only help industries save the chemical cost, but also provide them with the more accurate scale management strategy.

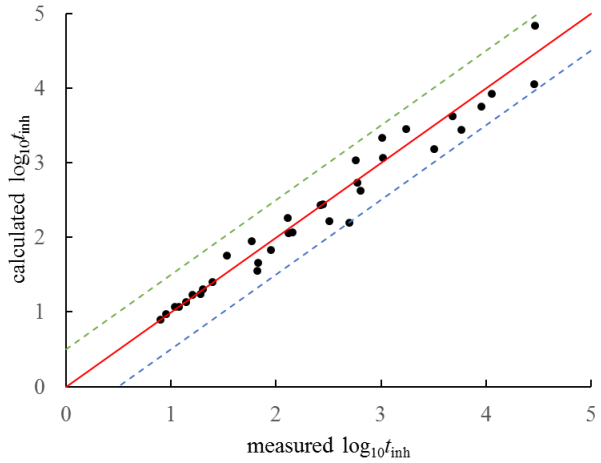

Figure 6: Evaluation of barite inhibition model with PESA at the conditions of barite *SI* 1.7 to 2.1 and *T* 50 to 90°C conditions. Red solid line: $y = x$; Green dashed line: $y = x + 0.5$; Blue dashed line: $y = x - 0.5$. The linear fitting result of the black dots: $y = 0.9802x$, $R^2 = 0.9631$.

CONCLUSION

In this study, a barite crystallization and inhibition model is developed at geothermal production conditions. The model is established based on the induction time measurement results of barite at the conditions of *SI* 1.7 – 2.1, *T* 50°C to 90°C, 0.2 mol/L NaCl and 0.01 mol/L Ca^{2+} with the absence and presence of PESA. The experimental conditions are selected based on geothermal produced water composition analysis results in various geothermal wells in China, indicating the potential of applying this model to geothermal productions. With this model, the severity of the barite scale problem and the inhibitor dosage needed can be predicted in advance, leading to a better scale management strategy for geothermal industry.

ACKNOWLEDGEMENT

This work was financially supported by SINOPEC Research Project (322051).

REFERENCES

Bozau, E., Häubler, S., and Van Berk, W.: Hydrogeochemical Modelling of Corrosion Effects and Barite Scaling in Deep Geothermal Wells of the North German Basin Using PHREEQC and PHAST, *Geothermics*, **53**, (2015), 540–547.

Bracco, J.N., Gooijer, Y., and Higgins, S.R.: Hydrothermal Atomic Force Microscopy Observations of Barite Step Growth Rates as a Function of the Aqueous Barium-to-Sulfate Ratio, *Geochimica et Cosmochimica Acta*, **183**, (2016), 1–13.

Cowan, J.C., and Weintritt, D.J.: Water-Formed Scale Deposits, *Gulf Publishing Company*, *Book Division*, (1976).

Dai, C., Dai, Z., Zhang, F., Zhao, Y., Deng, G., Harouaka, K., Wang, X., Lu, Y.T., Paudyal, S., Ko, S., Gao, S., Kan, A.T., and Tomson, M.B.: A Unified Experimental Method and Model for Predicting Scale Inhibition, *SPE International Symposium on Oilfield Chemistry*, (2019).

Dai, C., Paudyal, S., Ko, S., Ouyang, B., Lu, A. Y. T., Deng, G., Zhao, Y., Wang, X., Mateen, S., Kan, A.T., and Tomson, M.B.: A New Kinetic Turbidity Test Method for Calcite Scale Inhibition Study and Updates on Barite Scale Inhibition Model, *SPE International Oilfield Scale Conference and Exhibition*, (2020).

Dai, C., Stack, A.G., Koishi, A., Fernandez-Martinez, A., Lee, S.S., and Hu, Y.: Heterogeneous Nucleation and Growth of Barium Sulfate at Organic-Water Interfaces: Interplay between Surface Hydrophobicity and Ba^{2+} Adsorption, *Langmuir*, **32**, (2016), 5277–5284.

Dezayes, C., Genter, A., and Valley, B.: Structure of the Low Permeable Naturally Fractured Geothermal Reservoir at Soultz, *Comptes Rendus Geoscience*, **342**, (2010), 517–530.

Di Lorenzo, F., Cametti, G., Vanhecke, D., and Churakov, S.V.: The Role of Interfaces in Controlling Pb^{2+} removal by Calcium Carbonate Minerals, *Crystal Growth and Design*, **20**, (2020), 6157–6169.

Genter, A., Traineau, H., Dezayes, C., Elsass, P., Ledesert, B., Meunier, A., and Villemin, T.: Fracture Analysis and Reservoir Characterization of the Granitic Basement in the HDR Soultz Project (France), *International Journal of Rock Mechanics and Mining Sciences & Geomechanics Abstracts*, **33**, (1996), A69.

Griffiths, L., Heap, M.J., Wang, F., Daval, D., Gilg, H.A., Baud, P., Schmittbuhl, J., and Genter, A.: Geothermal Implications for Fracture-Filling Hydrothermal Precipitation, *Geothermics*, **64**, (2016), 235–245.

He, S., Oddo, J. E., and Tomson, M. B.: The Inhibition of Gypsum and Barite Nucleation in NaCl Brines at Temperatures from 25 to 90 °C, *Applied Geochemistry*, **9**, (1994), 561–567.

He, S., Kan, A.T., and Tomson, M.B.: Mathematical Inhibitor Model for Barium Sulfate Scale Control, *Langmuir*, **12**, (1996), 1901–1905.

Huang, X., Li, C., Zuo, K., and Li, Q.: Predominant Effect of Material Surface Hydrophobicity on Gypsum Scale Formation, *Environmental Science and Technology*, **54**, (2020), 15395–15404.

Kan, A.T., and Tomson, M.B.: Scale Prediction for Oil and Gas Production, *SPE Journal*, **17**, (2012), 362–378.

Kowacz, M., Putnis, C.V., and Putnis, A.: The Effect of Cation:Anion Ratio in Solution on the Mechanism of Barite Growth at Constant Supersaturation: Role of the Desolvation Process on the Growth Kinetics, *Geochimica et Cosmochimica Acta*, **71**, (2007), 5168–5179.

Oddo, J.E., and Tomson, M.B.: Why Scale Forms in the Oil Field and Methods to Predict It, *SPE Production & Facilities*, **9**, (1994), 47–54.

Orywall, P., Drüppel, K., Kuhn, D., Kohl, T., Zimmermann, M., and Eiche, E.: Flow-through Experiments on the Interaction of Sandstone with Ba-Rich Fluids at Geothermal Conditions, *Geothermal Energy*, **5**, (2017).

Peiris, R.H., Jaklewicz, M., Budman, H., Legge, R.L., and Moresoli, C.: Assessing the Role of Feed Water Constituents in Irreversible Membrane Fouling of Pilot-Scale Ultrafiltration Drinking Water Treatment Systems, *Water Research*, **47**, (2013), 3364–3374.

Pina, C.M., Becker, U., Risthaus, P., Bosbach, D., and Putnis, A.: Molecular-Scale Mechanisms of Crystal Growth in Barite, *Nature*, **395**, (1998), 483-486.

Risthaus, P., Bosbach, D., Becker, U., and Putnis, A.: Barite Scale Formation and Dissolution at High Ionic Strength Studied with Atomic Force Microscopy, *Colloids and Surfaces A: Physicochemical and Engineering Aspects*, **191**, (2001), 201–214.

Sánchez-Pastor, N., Pina, C.M., Fernández-Díaz, L., and Astilleros, J.M.: The Effect of CO_3^{2-} on the Growth of Barite {0 0 1} and {2 1 0} Surfaces: An AFM Study, *Surface Science*, **600**, (2006), 1369–1381.

Söhnel, O., and Mullin, J.W.: Interpretation of Crystallization Induction Periods, *Journal of Colloid and Interface Science*, **123**, (1988), 43–50.

Tranter, M., De Lucia, M., and Kühn, M.: Numerical Investigation of Barite Scaling Kinetics in Fractures, *Geothermics*, **91**, (2021).

Xiao, J., Kan, A.T., and Tomson, M.B.: Prediction of $BaSO_4$ Precipitation in the Presence and Absence of a Polymeric Inhibitor: Phosphino-Polycarboxylic Acid, *Langmuir*, **17**, (2001), 4668–4673.

Yan, C., Kan, A.T., Zhang, F., Liu, Y., Tomson, R.C., and Tomson, M.B.: Systematic Study of Barite Nucleation and Inhibition with Various Polymeric Scale Inhibitors by Novel Laser Apparatus, *SPE Journal*, **20**, (2015), 642–651.

Zhang, T., Gregory, K., Hammack, R.W., and Vidic, R.D.: Co-Precipitation of Radium with Barium and Strontium Sulfate and Its Impact on the Fate of Radium during Treatment of Produced Water from Unconventional Gas Extraction, *Environmental Science and Technology*, **48**, (2014), 4596–4603.

Zhang, Z., Zhang, P., Li, Z., Kan, A.T., and Tomson, M.B.: Laboratory Evaluation and Mechanistic Understanding of the Impact of Ferric Species on Oilfield Scale Inhibitor Performance, *Energy and Fuels*, **32**, (2018), 8348–8357.